Junli Xu*, Jing Zhang and Zhongning Shi

Extracting Aluminum from Aluminum Alloys in $AlCl_3$-NaCl Molten Salts

Abstract: Extracting aluminum from aluminum alloys in $AlCl_3$-NaCl molten salts was investigated in this paper. The influences of experimental parameters such as electrolyte composition, cathodic current density and electrolysis time on the deposits morphology were discussed. The results show that the grain size of the deposits decreases with the increase of $AlCl_3$ content in the electrolyte. Current density has a big effect on the morphology of the deposits. The particle size of deposits increases with the increase of current density, and dendritic morphology forms at high current density. High nucleation rates are achieved at high current densities above the limiting diffusion current density, and will result in a finer grain size. A non-dendritic deposit of aluminum was obtained at 170°C at 50 mA·cm^{-2} cathodic current density for 1 h in the electrolyte having a 1.3 molar ratio of $AlCl_3$/NaCl. The purity of the aluminum deposit is about 99.79% analyzed using inductively coupled plasma.

Keywords: aluminum extraction, recycling, aluminum alloy, chlorides

PACS® (2010). 82.45.Qr

***Corresponding author: Junli Xu:** School of Science, Northeastern University, Shenyang 110004, China. E-mail: jlxu@mail.neu.edu.cn
Jing Zhang: Huatian Engineering and Technology Corporation, MMC, Maanshan 243005, China
Zhongning Shi: School of Materials and Metallurgy, Northeastern University, Shenyang 110004, China

1 Introduction

Aluminum alloys are used extensively in structural and automotive applications. Due to the increased use of aluminum alloys, an increased amount of Al scrap has been generated. Aluminum recycling gains lots of attention based on the sustainable development and considering ecological and economic issues. Recycling aluminum alloys is both cost effective and environmentally friendly. It was reported that recycling aluminium requires only 5% of the energy and produces only about 4% of the CO_2 emissions as compared with primary production from the raw material bauxite and reduces the waste going to landfill [1–2].

Al scraps destined for recycling are usually categorized as new scrap and old scrap. New scrap is surplus material that arises during the manufacture and fabrication of aluminium alloys within the aluminium and manufacturing industry. This scrap is usually of known quality and composition. It is mainly recycled by remelters, which are generally integrated into rolling mills and extrusion plants. Old scrap originates from the end-of-life of final products, such as beverage cans, car cylinder heads, window frames from demolished buildings or old electrical cabling. Since there are hundreds of aluminum alloys developed for different purposes, most of the old scrap is usually collected without knowing the composition. It is clearly not very efficient to recycle old scrap by simple re-melting of unsorted waste metal. Sorting of aluminum alloys is a key factor for optimum recycling [3, 4]. Moreover, although aluminum alloys can be recycled, it is challenging for direct reusing of recycled aluminum alloys in wrought alloys or in cast alloys since some elements are up-limited in the recycled aluminum alloy [5, 6]. Most recycled aluminum has to be adjusted with more costly and energy-intense primary metal before it is reused in order to meet the performance requirements of most alloy and product specifications. There is a low demand amongst manufacturers for the direct recycled aluminum alloys, which cause processing plants to have a low interest in recycling such alloys.

In response to these problems, processes have been developed to extract pure aluminum from aluminum alloy scrap material so that the recycled aluminum may be utilized for other purposes. However, only a few works on the extraction of pure aluminum from aluminum alloys have been reported. Coldwell and Spendlove [7] reported using molten zinc to extract aluminum from aluminum-silicon alloys by the reflux leaching method. However, aluminum obtained by this method contains 1 to 6 percent silicon, 0.04 to 0.8 percent iron, and 0.01 to 0.9 percent titanium. The leached aluminum can only serve as a base alloy for producing sand-casting alloys.

Chloroaluminate ionic liquids are widely used for electrodeposition of aluminum and aluminum alloys

[8–27]. R.G. Reddy and co-workers reported recycling aluminum from aluminum alloy and aluminum metal matrix composite by electrolysis in ionic liquids [20–26]. High purity aluminum (99.89%) deposits were obtained on copper or aluminum substrates with a high current efficiency (>98%) [22]. They reported that this process has advantage of low energy consumption compared to the existing industrial aluminum refining process. The energy consumption for recycling pure aluminum in their studies was about 3–7 kWh/kg-Al [22, 23, 26].

Compared with ionic liquids, inorganic molten salts have higher electrical conductivity. Electroplating of aluminum or aluminum alloys has been investigated in alkali chloroaluminate melts [28, 29]. However, to the authors' knowledge, the extraction of aluminum from aluminum alloy in alkali chloroaluminate melts hasn't been reported yet. The objective of this work is to demonstrate the possibility for the aluminum extraction process from aluminum alloy in $AlCl_3$-NaCl molten salts, and to understand the mechanism of nucleation by electrochemical measurements.

2 Experimental

All the tests were performed in a 100 ml glass beaker fitted with a Teflon cap, and experiments were conducted with a three-electrode system using autolab PGSTAT30. For cyclic voltammetry tests, the working electrode was a Cu plate, and the counter electrode was a Pt plate to avoid disturbing the anodic dissolution reaction. For the electrodeposition process, aluminum alloy (6063 type) and Cu plates were used as the anode and cathode. The interpolar distance was about 3 cm. A pure aluminum wire was used as reference electrode for all tests. All of the electrolyte components were dried before use.

The deposits obtained on the cathode plate were stripped off from the substrate, and were washed in water by ultrasonic and dried at room temperature. The deposits structures were examined by scanning electron microscopy (SEM, JSM/6301F) and the phase of the deposits was characterized by a Rigaku D/MAX-3B X-ray diffractometer (XRD), with Cu Kα radiation. The impurities contents in the electrolyte were analyzed using IRISHR inductively coupled plasma (ICP).

3 Results and discussion

3.1 Electrode behavior in $AlCl_3$-NaCl molten salts

$AlCl_3$-NaCl melts exhibit Lewis acid-base properties. When $AlCl_3$ is mixed with NaCl, the ionic constituents of the resultant ionic liquid are determined by the mole ratio of $AlCl_3$/NaCl (q/p).

$$q\ AlCl_3 + p\ NaCl = q\ NaAlCl_4 + (p - q)\ NaCl \quad (q/p < 1) \tag{1}$$

$$q\ AlCl_3 + p\ NaCl = (2p - q)\ NaAlCl_4 + (q - p)\ NaAl_2Cl_7 \quad (1 < q/p < 2) \tag{2}$$

$Al_2Cl_7^-$ ion is a strong Lewis acid, while $AlCl_4^-$ ion is a Lewis base. The melts with $q/p > 1$ are acidic and those with $q/p < 1$ are basic, whereas the melt with $q/p = 1$ is neutral.

In our work, acidic melt was used to extract Al from Al alloy. Al alloy was used as anode, and Cu plate was used as cathode. During the extraction process, Al in the alloy anode dissolves into the melt.

$$Al + 7AlCl_4^- \rightarrow 4Al_2Cl_7^- + 3e \tag{3}$$

As there are two aluminum-containing complexes ($Al_2Cl_7^-$ and $AlCl_4^-$) in acidic melt, the cathodic deposition of aluminum at the cathode is possible by discharge of either of these two aluminum-containing complexes.

$$4Al_2Cl_7^- + 3e^- \rightarrow Al + 7AlCl_4^- \tag{4}$$

$$AlCl_4^- + 3e- \rightarrow Al + 4Cl^- \tag{5}$$

Figure 1 is the cyclic voltammetry curves at various n_{AlCl_3}/n_{NaCl} (1.1, 1.3, 1.5) with the scan rate of 0.1 V/s at 170°C. From Fig. 1a we can see that there are two reduction peaks and two oxidation peaks accordingly. By comparing Fig. 1(a)–(c), we can see that the position and shape of peaks are sensitive to the electrolyte composition. The peak of A becomes larger, and the peak of B becomes smaller with the increased content of $AlCl_3$ in the electrolyte. Since $Al_2Cl_7^-$ concentration in the electrolyte increases with the increase of n_{AlCl_3}/n_{NaCl}, while $AlCl_4^-$ concentration decreases with the increase of n_{AlCl_3}/n_{NaCl}, it is reasonable to induce that the reduction peak at –0.2 V potential (peak A) is due to the reduction of $Al_2Cl_7^-$ to Al, and the reduction peak at about –0.6 V potential (peak B) is due to the reduction of $AlCl_4^-$ to Al as equaction (4) and (5) show. The results are consistent with the conclusion that the

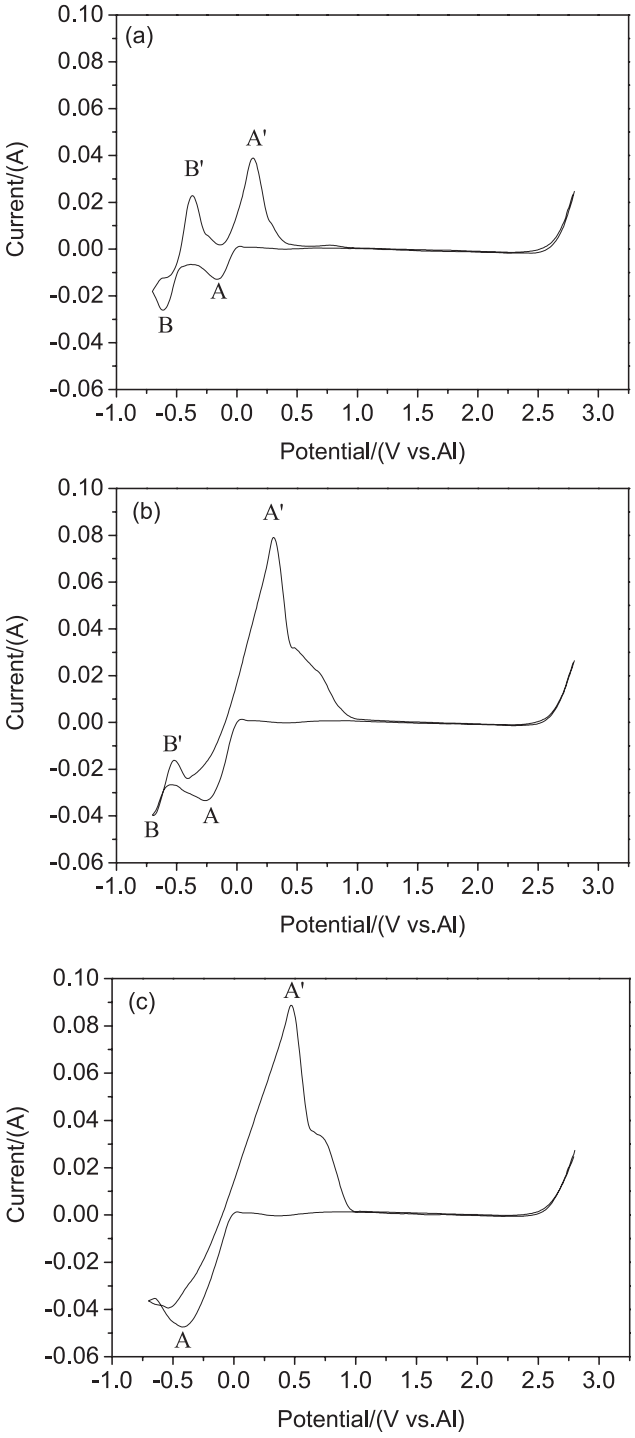

Fig. 1: Cyclic voltammograms recorded on W electrode in different molar ratio $AlCl_3$-NaCl molten salts at 170°C. Scan rates: 0.1 V/s. (a) $n_{AlCl_3}/n_{NaCl} = 1.1$; (b) $n_{AlCl_3}/n_{NaCl} = 1.3$; (c) $n_{AlCl_3}/n_{NaCl} = 1.5$.

deposition reaction is due to the discharge of $AlCl_4^-$ anions in a basic melt, while it is the $Al_2Cl_7^-$ anion which is reduced to give the aluminum deposit in an acidic melt [29, 30].

3.2 Effect of applied current density on the deposits microstructure

Figure 2 shows the microstructure of the deposits at different cathodic current density. As seen in Fig. 2, the microstructures are spherical varying in the size from 5 μm to about 10 μm for the deposits which are obtained at 25 and 50 $mA \cdot cm^{-2}$ while it was dendritic when the current density is 75 $mA \cdot cm^{-2}$. However, with further increase of current density (at 100 $mA \cdot cm^{-2}$), the microstructure is spherical again. As we know, the nature and morphology of the deposit are influenced by the rate of the electron transfer reaction and concentration. The nucleation rate depends on the current density, which governs the driving force for crystallization. The charge-transfer rate is very slow at 25 $mA \cdot cm^{-2}$, which result in few nuclei, low growth rate. With the increase of deposition current density, the nucleation rate and growth rate increase which result in the increase of nuclei and micrograph size as Fig. 2(a) and (b) shown. With the further increase of current density, more new nuclei form at the same time, and the deposit shows a very rapid growth. This growth usually leads to whiskers and dendrites. This is because nuclei express the preferred growth directions of the crystal. This growth direction may be due to anisotropy in the surface energy of the solid–liquid interface, or to the ease of attachment of atoms to the interface on different crystallographic planes, or both which results in a dendritic nature of the deposit [31]. If the anisotropy is large enough, the dendrite may present a faceted morphology, as shown in Fig. 2(c). However, after the current density is larger than the limiting diffusion current density, lots of nuclei form simultaneously. At the same time, new nucleation process and the growth of the independent nuclei are almost terminated since the electroactive species is depleted near the cathode. After new electroactive species is transported to the cathode, the nucleation process takes place again. Thus, most deposited particles are in the same shape as Fig. 2(d) shown. Deposits exhibit a tendency to appear in the form of powders in this condition [32].

3.3 Effect of $AlCl_3$/NaCl molar ratio on the microstructure of deposits

As dendritic or powdery deposits may easily fall off the electrode, which will reduce current efficiency of the process, we choose 50 $mA \cdot cm^{-2}$ as the cathodic current density in the following experiments since it should be possible to obtain the spherical crystal with an acceptable reduction rate. The microstructures of the deposits

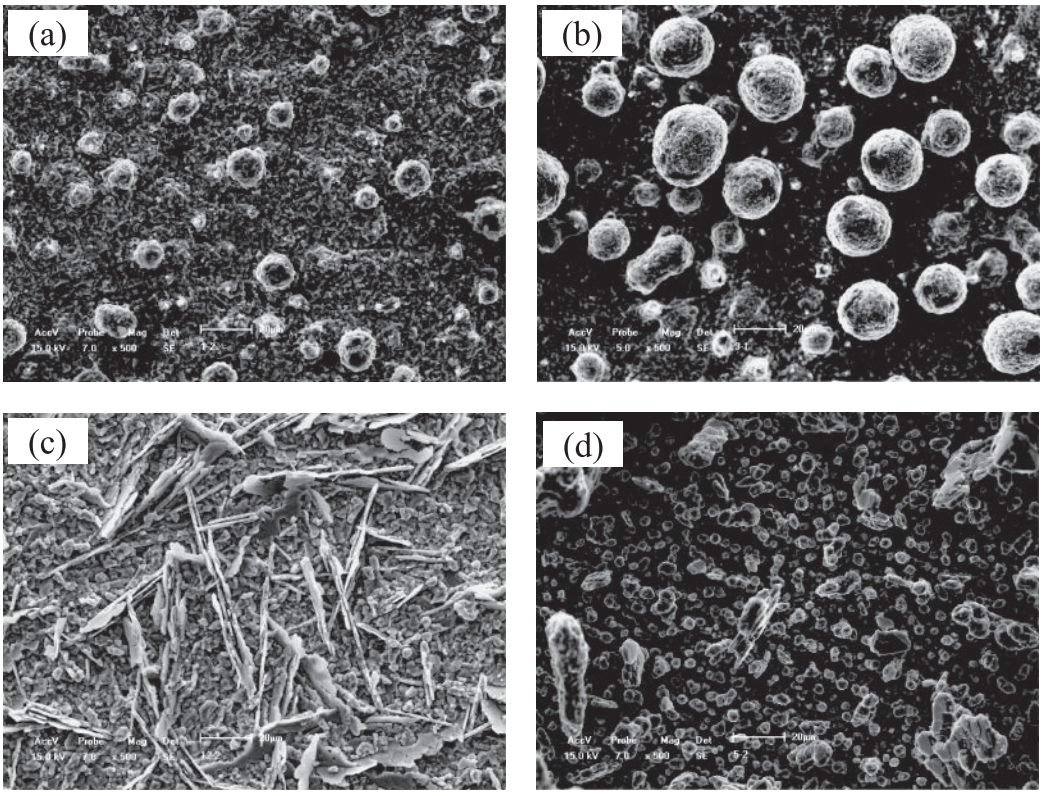

Fig. 2: SEM micrographs of aluminum electrodeposits prepared on Cu electrodes from 1.3:1 molar ratio $AlCl_3$-NaCl molten salts at 170°C for 0.5 h. The applied current densities are 25 mA·cm^{-2} (a), 50 mA·cm^{-2} (b), 75 mA·cm^{-2} (c) and 100 mA·cm^{-2} (d) respectively.

obtained at 50 mA·cm^{-2}, 170°C with different n_{AlCl_3}/n_{NaCl} are shown in Fig. 3. As can be seen the morphology of the deposit is sensitive to n_{AlCl_3}/n_{NaCl}. The grain size becomes smaller and denser with the increase of n_{AlCl_3}/n_{NaCl}. The grain size is in a close range of 15–20 μm when n_{AlCl_3}/n_{NaCl} is 1.3 and 1.5, while it is in a close range of 5–10 μm when n_{AlCl_3}/n_{NaCl} is 1.7 and 1.9.

According to the familiar Nernst equation (equation 6), electrodeposition of M can occur at potential which is more negative than the equilibrium potential E_M. This difference in potential is the overpotential (η^M).

$$E_M = E_M^{\vartheta} + (RT/nF)\ln[(\alpha_{M^{m+}})/\alpha_M] \quad (6)$$

where E_M^{ϑ} is the standard potentiall for the reduction to form M, R is the gas constant, T is the absolute temperature, m is the number of electrons required for the reduction, F is the Faraday constant, and $\alpha_{M^{m+}}$ and α_M are the activities of M^{m+} in the electrolyte, and of M in the deposit, respectively. The number of nuclei is strongly dependent on the overpotential. The more positive of E_M value, the easier it is to reduce metal ions, and the more negative of E_M value, the more difficult it is to reduce the metal ions.

$Al_2Cl_7^-$ concentration increases with the increase of n_{AlCl_3}/n_{NaCl}, which results in the increase of the equilibrium potential E_M. Thus, the overpotential decreases with the increase of n_{AlCl_3}/n_{NaCl} since the applied current density is kept constant. If the nucleation process is driven by electron transfer process, a lower amount of nuclei and larger grains will be obtained with the decrease of overpotential. However, the results are not the same. The grain size becomes smaller and denser with the increase of n_{AlCl_3}/n_{NaCl} at the experimental condition. The result suggests that the nucleation process at the carried condition is driven by diffusion process, and the actual current density is larger than the limiting current density. The nucleation rate at the applied current density is very quick. Higher concentration of active ion results in the higher amount of nuclei and therefore smaller grains.

3.4 Effect of electrolysis time on the microstructure of deposits

Figure 4 shows the microstructures of aluminum deposits obtained at constant current density 25 mA·cm^{-2},

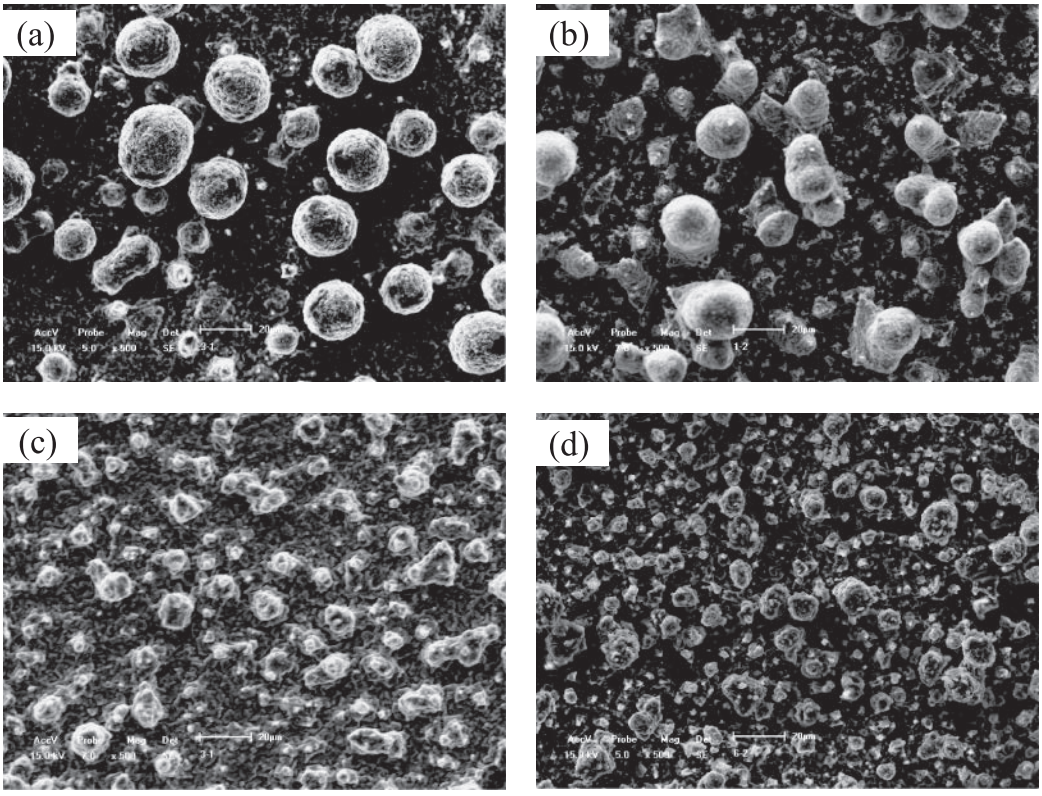

Fig. 3: SEM micrographs of aluminum electrodeposits prepared on Cu electrodes in different molar ratio $AlCl_3$-NaCl molten salts at constant current density 50 mA·cm^{-2} for 0.5 h at 170°C. (a) $n_{AlCl_3}/n_{NaCl} = 1.3$; (b) $n_{AlCl_3}/n_{NaCl} = 1.5$; (c) $n_{AlCl_3}/n_{NaCl} = 1.7$; (d) $n_{AlCl_3}/n_{NaCl} = 1.9$.

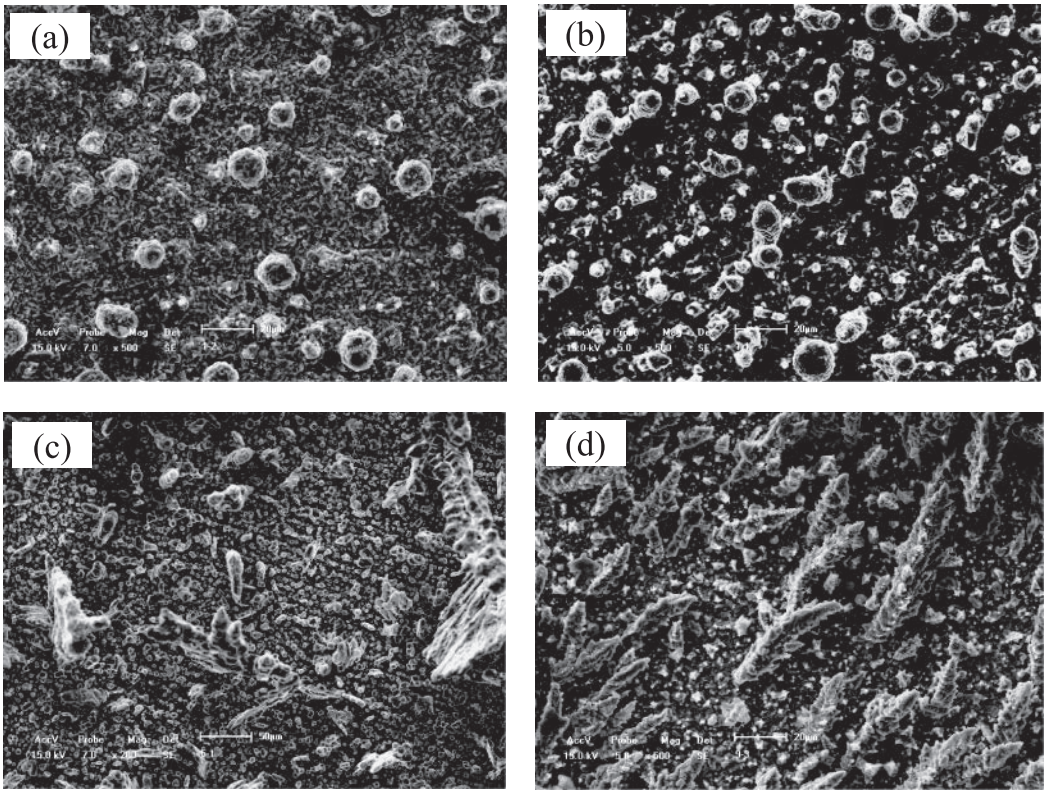

Fig. 4: SEM micrographs of aluminum electrodeposits prepared on Cu electrodes in 1.3:1 molar ratio $AlCl_3$-NaCl molten salts using 25 mA·cm^{-2} current density at 170°C for different electrolysis time. The electrolysis time is 0.5 h (a), 1 h (b), 1.5 h (c) and 2 h (d) respectively.

Component	Si	Fe	Mg	Cu	Mn	Cr	Zn	Ti	Al
Content	0.059	0.011	0.128	<0.001	<0.001	0.004	0.001	0.001	99.794

Table 1: Composition of the deposited aluminum (mass fraction %)

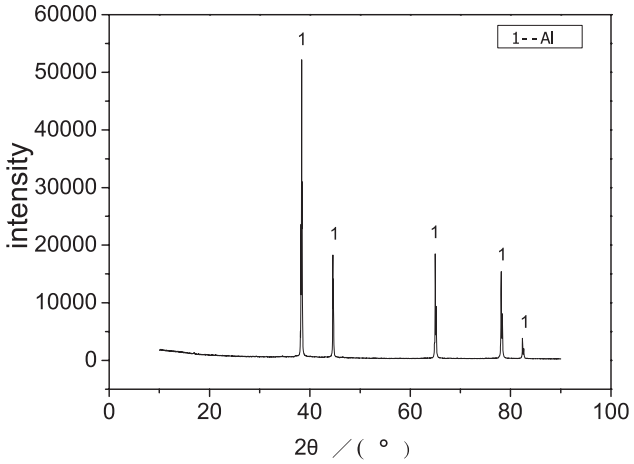

Fig. 5: X-ray diffraction pattern of aluminum deposit

$n_{AlCl_3}/n_{NaCl} = 1.3$ and temperature 170°C for different electrodeposition time. It can be seen that a uniform deposit of spherical particles can be observed with 0.5–1 h deposition time, while the microstructure of the aluminum deposits became dendritic-like after prolong the deposition time. Preferred orientation growth induces the dendritic-like microstructure formation.

3.5 Purity of the deposited aluminum

The deposit gained at 50 mA·cm^{-2} with $n_{AlCl_3}/n_{NaCl} = 1.3$ at 170°C for 4 h was taken off from the copper cathode surface and analyzed by XRD and ICP. The results are shown in Fig. 5 and Table 1. The XRD result shows there is only Al exiting in the deposit. The purity of the aluminum deposit is about 99.8%. The impurities are mainly Si, Mg and Fe, which come from the anode.

4 Conclusions

High purity aluminum (about 99.8%) was successfully reclaimed from aluminum alloy by electrolysis in $AlCl_3$-NaCl molten salts. The electrolyte composition, cathodic current density and deposition time have great effects on the microstructures of the aluminum deposits. With the increase of $AlCl_3$/NaCl mole ratio, the deposits particle size decreases. Long deposition time results in the formation of dendritic morphology. The dependency of the morphology on the current density is attributed to the change in the deposition rate. Low current density results in less nucleation and growth rate. Hence the particle size increases with increase of current density, and dendritic morphology formed at high current density. However, high nucleation rates achieved at high current density which is above of limiting diffusion current density resulted in a finer grain size.

Acknowledgement: The authors gratefully acknowledge the financial support from the national natural science foundation of China (No. 51104042).

Received: October 13, 2012. Accepted: November 24, 2012.

References

[1] S.K. Das, Light metals 2006, 911–916.
[2] S.K. Das, W. Yin, JOM, 59(11) (2007) 57–63.
[3] V. Kevorkijan, JOM, 54(02) (2002) 38–41.
[4] S.K. Das, Materials Science Forum, 519–521 (2006) 1239–1244.
[5] J.B. Hess, Metallurgical Transactions A, 14 (1983) 323–327.
[6] J. Cui, H.J. Roven, Trans. Nonferrous Met. Soc. China, 20 (2010) 2057–2063.
[7] H.S. Coldwell, M.J. Spendlove, United States Department of the Interior Bureau of Mines, 1961.
[8] P.K. Lai, M. Skyllas-Kazacos, Electrochimica Acta, 32 (1987) 1443–1449.
[9] P.K. Lai, M. Skyllas-Kazacos, Journal of Electroanalytical Chemistry and Interfacial Electrochemistry, 248 (1988) 431–440.
[10] C.C. Yang, Materials Chemistry and Physics, 37 (1994) 355–361.
[11] Q. Liao, W.R. Pitner, G. Stewart, C.L. Hussey, and G.R. Stafford, Journal of the Electrochemical Society, 144 (1997) 936–943.
[12] Y. Zhao, T.J. VanderNoot, Electrochimica Acta, 42 (1997) 1639–1643.
[13] H. Lu, Y. Wang, Z. Liu, X. Zhai, J. Liu, T. Hong, Light Metals, 2006, 319–322.
[14] L.P. Zhang, X.J. Yu, Y.H. Dong, D.G. Li, Y.L. Zhang, Z.F. Li, Trans. Nonferrous Met. Soc. China, 20 (2010) s245–s248.
[15] T. Jiang, M.J. Chollier Brym, G. Dube, A. Lasia, G.M. Brisard, Surface and Coatings Technology, 201 (2006) 1–9.
[16] T. Jiang, M.J. Chollier Brym, G. Dube, A. Lasia, G.M. Brisard, Surface and Coatings Technology, 201 (2006) 10–18.
[17] J.K. Chang, S.Y. Chen, W.T. Tsai, M.J. Deng, I.W. Sun, Electrochemistry Communications, 9 (2007) 1602–1606.

[18] T. Tsuda, T. Nohira, Y. Ito, Electrochimica Acta, 47 (2002) 2817–2822.
[19] U. Bardi, S. Caporali, M. Craig, A. Giorgetti, I. Perissi, J.R. Nicholls, Surface and Coatings Technology, 203 (2009) 1373–1378.
[20] B. Wu, R.G. Reddy, R.D. Rodegers, The Fourth International Symposium on Recycling of Metals and Engineered Materials. Warrendale, PA: TMS, 2000: 845–856.
[21] R.G. Reddy, Metallurgical and Materials Transactions B, 34 (2003) 137–152.
[22] V. Kamavaram, D. Mantha, R.G. Reddy, J. Mining and Metallurgy, 39(1–2)B (2003) 43–58.
[23] V. Kamavaram, D. Mantha, R.G. Reddy, Electrochimica Acta, 50 (2005) 3286–3295.
[24] M. Zhang, V. Kamavaram, R.G. Reddy, Minerals and Metallurgical Processing, 23 (2006) 177–186.
[25] D. Pradhan, D. Mantha, R.G. Reddy, Electrochimica Acta, 54 (2009) 6661–6667.
[26] D. Pradhan, R.G. Reddy, Metallurgical and Materials Transactions B, 43B (2012) 519–531.
[27] D. Pradhan, R.G. Reddy, Electrochimica Acta, 54 (2009) 1874–1880.
[28] K. Grjotheim, K. Matiasovsky, Acta Chemica Scandinavica A, 34 (1980) 666–670.
[29] G.R. Stafford, G.M. Haarberg, Plasmas & Ions, 1 (1999) 35–44.
[30] Q.F. Li, Z.X. Qiu, Applied electrochemistry of aluminum-production and applications, Northeastern University Publisher, Shenyang, 2003: 138–144.
[31] T. Devers, I. Kante, L. Allam, V. Fleury, J. Non-Crystalline Solids, 321 (2003) 73–80.
[32] K.I. Popov, S.S. Djokic, B.N. Grgur, Fundamental aspects of electrometallurgy, Kluwer Academic Publishers, New York, 2002: 89–92.